Proc. Natl. Acad. Sci. USA
Vol. 92, pp. 11578–11582, December 1995
Biochemistry

Projection structure of frog rhodopsin in two crystal forms

GEBHARD F. X. SCHERTLER* AND PAUL A. HARGRAVE†

Medical Research Council Laboratory of Molecular Biology, Hills Road, Cambridge, CB2 2QH, United Kingdom

Communicated by Aaron Klug, Medical Research Council Laboratory of Molecular Biology, Cambridge, United Kingdom, May 24, 1995

ABSTRACT **Rhodopsin is the G protein-coupled receptor that upon light activation triggers the visual transduction cascade. Rod cell outer segment disc membranes were isolated from dark-adapted frog retinas and were extracted with Tween detergents to obtain two-dimensional rhodopsin crystals for electron crystallography. When Tween 80 was used, tubular structures with a $p2$ lattice (a = 32 Å, b = 83 Å, γ = 91°) were formed. The use of a Tween 80/Tween 20 mixture favored the formation of larger $p22_12_1$ lattices (a = 40 Å, b = 146 Å, γ = 90°). Micrographs from frozen hydrated frog rhodopsin crystals were processed, and projection structures to 7-Å resolution for the $p22_12_1$ form and to 6-Å resolution for the $p2$ form were calculated. The maps of frog rhodopsin in both crystal forms are very similar to the 9-Å map obtained previously for bovine rhodopsin and show that the arrangement of the helices is the same. In a tentative topographic model, helices 4, 6, and 7 are nearly perpendicular to the plane of the membrane. In the higher-resolution projection maps of frog rhodopsin, helix 5 looks more tilted than it appeared previously. The quality of the two frog rhodopsin crystals suggests that they would be suitable to obtain a three-dimensional structure in which all helices would be resolved.**

Bovine rhodopsin, the light-absorbing receptor protein found in disc membranes in the outer segments of rod cells (1, 2), was the first G protein-coupled receptor whose sequence was determined (3–5). Primary sequence homology of 31 vertebrate and 16 invertebrate opsins (1) with other G protein-coupled receptors suggests that their three-dimensional structures are likely to be similar as well (6, 7). Characteristic features of rhodopsin shared by most G protein-coupled receptors include asparagine-linked oligosaccharide attachment sites in the amino-terminal region (8), palmitate-linked cysteines in the carboxyl-terminal region (9, 10), serine and threonine phosphorylation sites in the carboxyl-terminal region (1), and a disulfide bridge (11, 12). The light sensitivity of rhodopsin is mediated by 11-*cis*-retinal bound to a lysine side chain of the seventh helix by a Schiff base linkage (13). Other members of the G protein-coupled receptor family are believed to bind ligands in a pocket formed by the interior surface of the transmembrane helices (14). Physical studies of rod outer segment membranes have shown rhodopsin to be a transmembrane protein with approximately half of the mass embedded in the hydrophobic portion of the lipid bilayer. The remaining mass is equally distributed between the two hydrophilic surfaces exposed on each side of the membrane (15). α-Helices which comprise 50% of rhodopsin's structure (16) appear to be arranged roughly perpendicular to the plane of the membrane (17). Chemical modification, protease digestion, lectin and antibody binding, and site-directed mutagenesis studies support a topographic model in which the amino terminus of rhodopsin is on the intradiscal membrane surface, the carboxyl terminus is exposed to the cytoplasmic surface, and the polypeptide traverses the membrane seven times, burying seven hydrophobic α-helices and exposing hydrophilic interhelical regions (3, 5). Direct evidence for the arrangement of the α-helices in rhodopsin was obtained from a 9-Å projection structure of bovine rhodopsin. The resolution of the map revealed an arc-shaped feature accounting for three tilted helices and four resolved peaks interpreted as transmembrane helices oriented nearly perpendicular to the membrane (18). Structural constraints obtained from sequence analysis of G protein-coupled receptor sequences have been used to allocate particular helices to the peaks in the projection map of bovine rhodopsin, and a three-dimensional arrangement of the helices has been proposed (6).

In this paper we present two projection maps of frog rhodopsin at significantly higher resolution. At the current resolution helix 5 appears more tilted than expected previously. Our results further support the proposal that the position and orientation of the seven transmembrane helices of rhodopsin and bacteriorhodopsin are clearly distinct.

RESULTS

Crystallization of Frog Rhodopsin. Disc membranes prepared from dark-adapted frog retinas were extracted with Tween 80 at a variety of molar ratios to induce the formation of two-dimensional arrays of rhodopsin (19). Crystals were observed at a molar ratio of 1000:1 between Tween 80 and rhodopsin. A time course of the extraction at a molar ratio of 1500:1 was followed by electron microscopy. In the best sample nearly 20% of the membranes were crystalline after 16 hr (Fig. 1*A*). Electron micrographs showed tubular structures with a $p2$ lattice growing from the disc membranes (Fig. 1 *A* and *C*). With Tween 20, Tween 40, and Tween 60 at a molar ratio of 1000:1 two-dimensional crystals were observed in all samples after 16 hr. With Tween 20 small crystals were formed, whereas combination of Tween 20 and Tween 80 at a ratio of 500:500:1 produced larger crystalline sheets composed of two superimposed $p22_12_1$ crystalline layers (Fig. 1 *B* and *D*).

Electron Cryomicroscopy and Image Processing. The crystal suspensions were applied to carbon-coated electron microscopy grids and frozen rapidly in liquid ethane (20). Electron micrographs were taken at liquid nitrogen temperature and inspected by optical diffraction. A diffraction pattern of a frog rhodopsin crystal obtained by extraction with a mixture of Tween 80 and Tween 20 indicated two superimposed orthorhombic lattices with a = 40 Å, b = 146 Å, and γ = 90° (Fig. 2*B*). Four images with sharp optical diffraction spots to 10-Å resolution were chosen for computer processing. Visual inspection of computer-averaged maps showed a set of twofold symmetry axes normal to the membrane plane and screw axes parallel to a and b which were also indicated by the systematic absence of odd reflections along the a and b axes. Phase relationships between Fourier components were examined with the program ALLSPACE (21) for several images. The appropriate internal phase residual was calculated in all 17 space groups for a single film. Phase residuals shown in Table 1 for lattice FRG259a exclude space group 7 corresponding to

The publication costs of this article were defrayed in part by page charge payment. This article must therefore be hereby marked "*advertisement*" in accordance with 18 U.S.C. §1734 solely to indicate this fact.

*To whom reprint requests should be addressed.
†Present address: University of Florida Department of Ophthalmology, School of Medicine, Gainesville, FL 32610-0284.

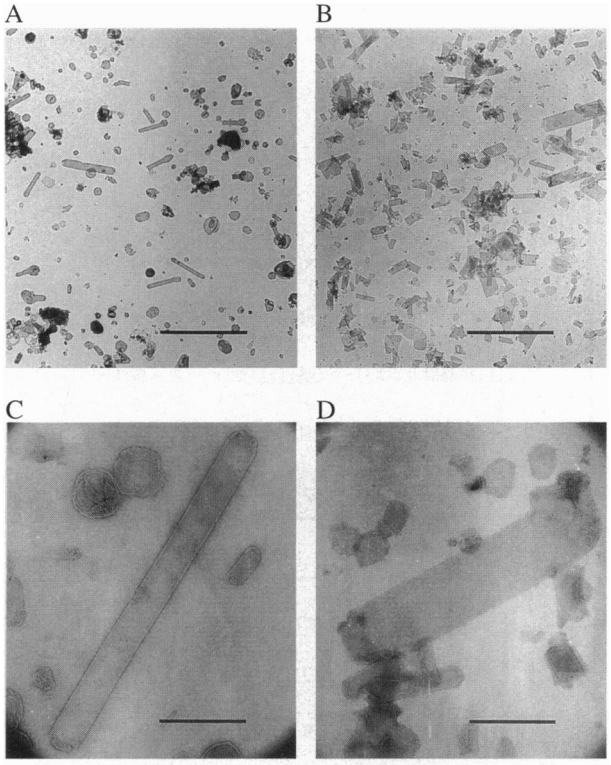

FIG. 1. Micrographs of frog disc membranes after Tween extraction. Frog disc membranes were incubated for 16 hr with Tween 80 or a mixture of Tween 80 and Tween 20 at a molar ratio of 1000:1 in Tes buffer (25 mM Tes/100 mM NaCl/0.1 mM dithiothreitol, pH 7.5), washed three times, resuspended in Tes buffer at a concentration of 1 mg of rhodopsin per ml, and stained with a 1% uranyl acetate solution. Crystals obtained by extraction with Tween 80 which contain rhodopsin in the $p2$ crystal form are shown in A and C, and $p22_12_1$ crystals are shown in B and D. [Bars = 5 μM (A and B) or 0.5 μM (C and D).]

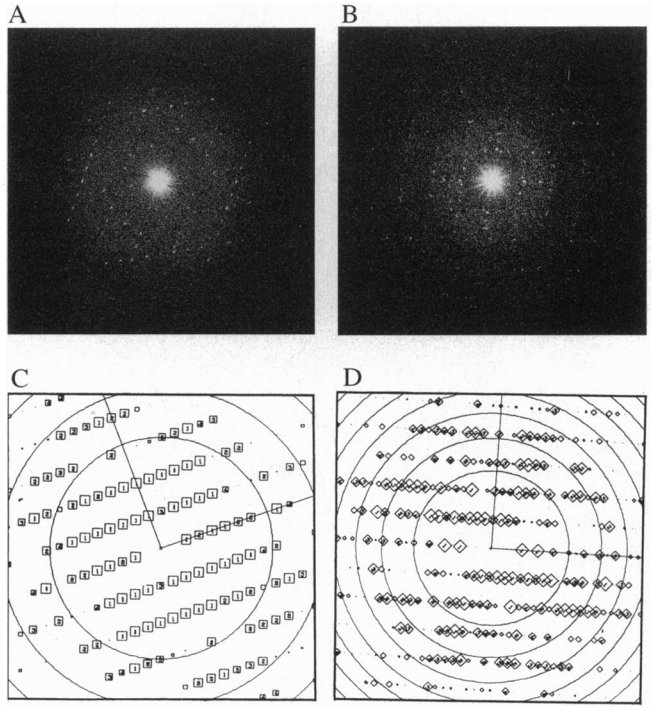

FIG. 2. Optical diffraction of frog rhodopsin crystals and Fourier transforms of distortion-corrected images. Crystals were rapidly frozen in liquid ethane, and electron micrographs were taken at liquid nitrogen temperature with a Gatan 626 cold stage and inspected by optical diffraction. In A the diffraction spots can be indexed on two independent $p2$ lattices with a = 32 Å, b = 83 Å, and γ = 91° for both layers. B shows a diffraction pattern of a frog $p22_12_1$ crystal. Two lattices can be indexed with a = 40 Å, b = 146 Å, and γ = 90°. Digitized areas (2000 × 2000 pixels at 10-μm intervals; Joyce–Loebl Mk4 densitometer) were corrected for distortions in the crystal lattice by using a 200 × 200-pixel reference area. In a second round a 150 × 150-pixel area from the corrected image was used as reference. In a third round an extended list of Fourier components as reference improved the higher-resolution components further. Finally, the crystalline area was boxed off before calculation of amplitudes and phases. C shows the output for a $p2$ crystal, and D for a $p22_12_1$ crystal.

$p222_1$. Good agreement of the phase residual for space group 8 with the target residual confirms the $p22_12_1$ symmetry of the crystals. Optical diffraction patterns of a frog rhodopsin crystal obtained by Tween 80 extraction showed two superimposed primitive lattices with a = 32 Å, b = 83 Å, and γ = 91° (Fig. 2A). From 150 micrographs the best seven images with sharp optical diffraction spots to 10-Å resolution were chosen for image processing. In computer-averaged $p1$ maps the only detectable symmetry was a set of twofold axes normal to the membrane plane. Phase relations calculated by ALLSPACE for the lattice FRG500a are shown in Table 1. They confirmed the $p2$ symmetry of the crystal lattice. The best crystalline areas of four images of $p22_12_1$ crystals were selected by optical diffraction and digitized. The two superimposed lattices were treated separately, giving a total of 8 crystals. Distortions in the crystal lattice were removed in an iterative three-step procedure using a progressively improved reference (22, 23). Finally, the precise extent of the crystal was boxed off before calculation of amplitudes and phases (24, 25). The two superimposed lattices of seven images of the $p2$ form were treated in the same way, giving a total of 14 crystals. The amplitudes obtained from one of the images of the $p22_12_1$ and the $p2$ form are shown in Fig. 2 D and C, respectively. The data from 8 crystalline areas of the $p22_12_1$ form were initially merged by using approximate contrast transfer function corrections and brought to the same amplitude scale. The phase origin and defocus of individual images were then iteratively refined. For each reflection the amplitude was corrected for the contrast transfer function and the structure factors were averaged vectorially. Finally, phases were rounded to either 0° or 180°, since the projection is centrosymmetric. The same was done for 14 crystalline areas of the $p2$ form. Comparison with 0° or 180° allowed statistical analysis of the phase accuracy (Tables 2 and 3). The phase errors of the unique Fourier components to 5 Å are plotted for one asymmetric unit in Fig. 3 A and B. Phases are reliable to 7-Å resolution for the $p22_12_1$ form and to 6 Å for the $p2$ form (Fig. 3; Tables 2 and 3). The fading of the image amplitudes is due to the limited intrinsic order in the crystals (Fig. 3C). The image amplitudes were rescaled as a function of resolution by applying a correction derived from a comparison with the average diffraction amplitude of bacteriorhodopsin. All procedures, including contrast transfer function correction, origin refinement, and rescaling were carried out as described (18, 24, 25).

Frog Rhodopsin $p22_12_1$ and $p2$ Projection Maps. From merged and scaled amplitudes and phases we have calculated a projection structure of frog rhodopsin at 7-Å resolution for the $p22_12_1$ form (Fig. 4A) and a map to 6-Å resolution for the $p2$ form (Fig. 4B). In the $p22_12_1$ map the twofold axes normal to the membrane plane and the screw axes parallel to the a and b axes are indicated; in the $p2$ form only a set of twofold axes normal to the membrane plane is present. By comparing the two maps it is easy to recognize the boundary of a single molecule. The packing in the two crystal forms is related, since in both crystals pairs of molecules pointing in the same direction are related by a twofold axis. However, in contrast to

Table 1. Internal phase residuals for seven space groups

	Space group	Phase residuals, degrees: Versus other spots (90 random)	Versus theoretical (45 random)	No. of spots	Target residual,* degrees
		Lattice FRG259a			
1	$p1$	28.3†	20.8†	156	
2	$p2$	36.3‡	18.1	156	41.7
3a	$p12a$	79.8	40.5	8	29.3
3b	$p12b$	64.8	37.4	14	29.9
4a	$p121a$	20.4‡	26.1	8	29.3
4b	$p121b$	28.0‡	9.9	14	29.9
6	$p222$	61.4	18.2	156	33.7
7a	$p222_1a$	64.4	39.5	156	33.7
7b	$p222_1b$	54.6	35.3	156	33.7
8	$p22_12_1$	29.1‡	18.1	156	33.7
		Lattice FRE500a			
1	$p1$	22.1†	16.0†	96	
2	$p2$	26.2‡	13.1	96	32.0
3a	$p12a$	67.2	47.2	6	23.0
3b	$p12b$	61.4	47.2	14	23.9
4a	$p121a$	51.5	47.2	6	23.0
4b	$p121b$	75.5	47.4	14	23.9
6	$p222$	75.7	43.5	96	26.1
7a	$p222_1a$	68.8	13.6	96	26.1
7b	$p222_1b$	45.2	13.3	96	26.1
8	$p22_12_1$	66.0	13.3	96	26.1

*Taking Friedel weight into account.
†Note that in space group $p1$ no phase comparisons are possible. The numbers given are theoretical phase residuals based on the signal-to-noise ratio of observed amplitudes.
‡As good as target phase residual.

the $p22_12_1$ form, in the $p2$ form all molecules are oriented in the same direction.

Comparison of Projection Maps of Frog and Bovine Rhodopsin. The total area per rhodopsin molecule is smallest in the frog $p2$ crystal (Table 4). The projection maps of frog rhodopsin are very similar to the projection obtained for bovine rhodopsin at 9-Å resolution (18). Distances between density peaks that can be identified in all three maps are

Table 2. Image statistics

	$p22_12_1$	$p2$
No. of images	4	7
No. of crystalline areas	8	14
Variation in cell parameters, %	±3	±2
Range of defocus, Å	4000–7000	1800–5800
Range of astigmatism	0–900	0–200
Total no. of reflections*	1763	1546
Total no. of unique reflections*	190	154
Overall phase residual†, degrees	33.0	27.5

Table 3. Resolution dependence of phase residual

Resolution range, Å	$p22_12_1$: No. of unique reflections	$p22_12_1$: Phase residual,† degrees	$p2$: No. of unique reflections	$p2$: Phase residual,† degrees
200.0–14.4	28	17.8	20	6.3
14.4–10.2	23	26.2	18	10.4
10.2–8.3	24	26.7	19	14.1
8.3–7.0	30	32.1	26	36.5
7.0–6.0	36	37.7	29	33.9
6.0–5.0	49	51.2	42	40.5

*For all data to 5-Å resolution.
†Compared with 0°/180°; 45° is a random value.

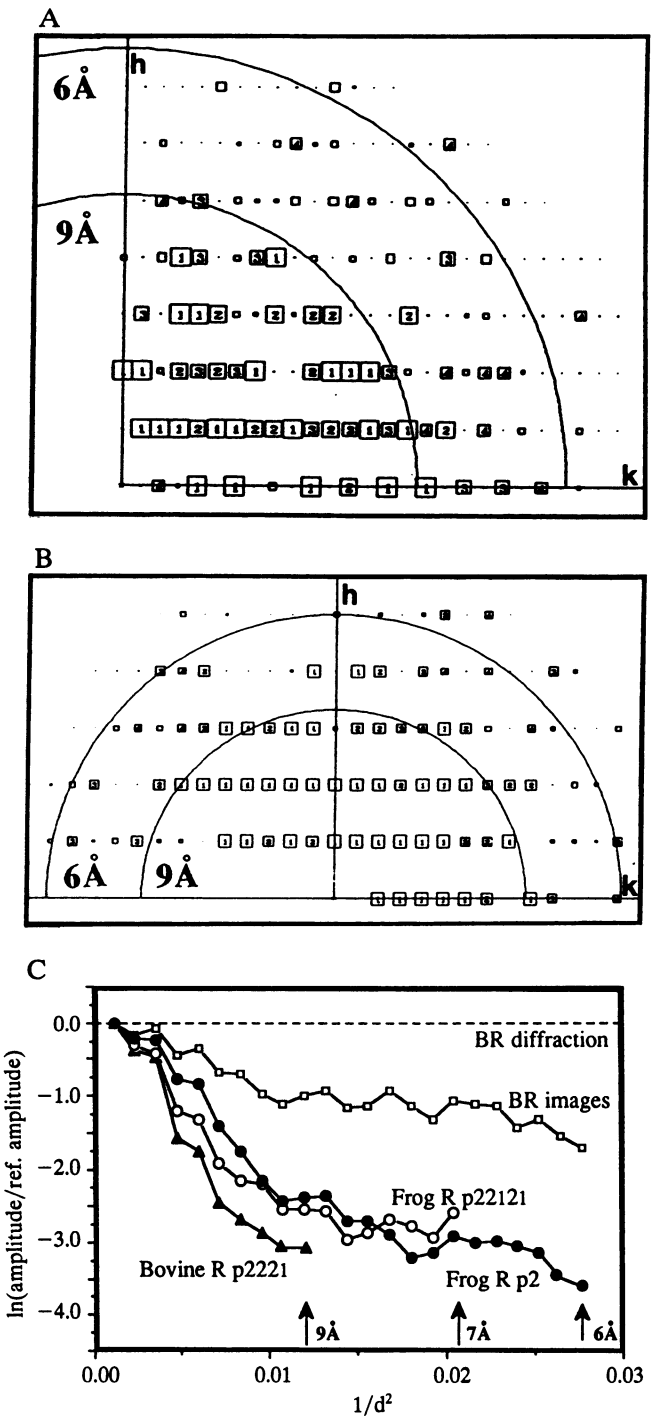

FIG. 3. Phase errors of unique Fourier components and resolution-dependent fading of image amplitudes. Unique Fourier components are plotted along the h and k axes. The size of the boxes indicates the phase error associated with each measurement before rounding of the phase to 0° or 180° (1, <8°; 2, <15°; 3, <22°; 4, <29°; 5, <36°; 6, <42°; 7, <57°; 8, <90°; values from 1–8 are indicated by decreasing box size). In this case, 90° is random. *A* and *B* show phase residuals for the $P22_12_1$ and $P2$ crystals, respectively. The ratio between average image amplitudes and average bacteriorhodopsin (BR) electron diffraction amplitudes in resolution zones was plotted against $1/d^2$ in *C*. The image amplitudes of frog and bovine rhodopsin (R) crystals were rescaled as a function of resolution, to compensate for the loss of contrast. The amplitude data from the frog $p2$ crystals fade more slowly and extend to higher resolution; although this rescaling used electron diffraction data from bacteriorhodopsin as a reference, similar rescaling is obtained when data from other proteins are used (18, 24, 25).

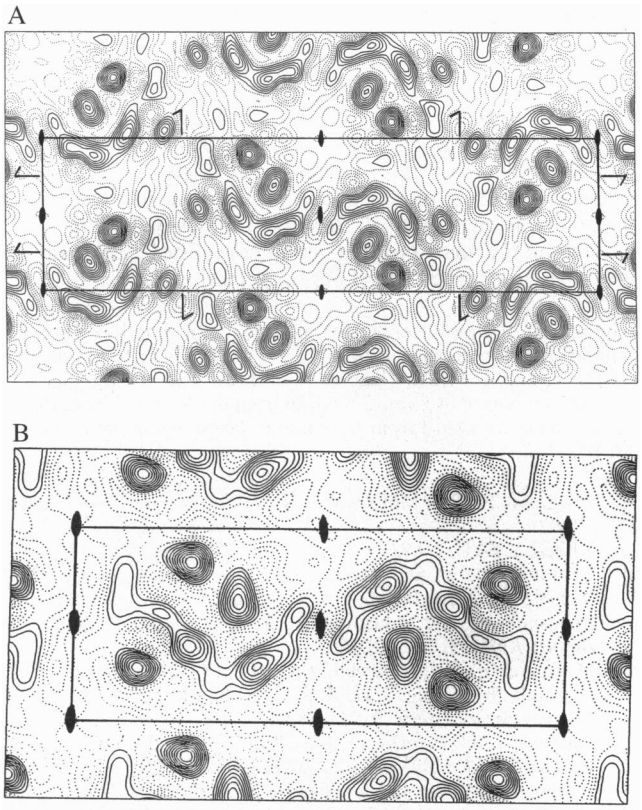

FIG. 4. Projection maps of frog rhodopsin. A map of rhodopsin to 7-Å resolution for the $p22_12_1$ crystals and to 6-Å resolution for the $p2$ form was calculated from merged and corrected image amplitudes and phases. A unit cell with the a axis vertical and the b axis horizontal is shown in A. The space group is $p22_12_1$ (a = 40 Å, b = 146 Å, γ = 90°). The twofold axes perpendicular to the membrane plane and the screw axes parallel to a and b are indicated. One unit cell contains four rhodopsin molecules. In B a unit cell containing two molecules is shown with the a axis vertical and the b axis horizontal ($p2$ a = 32 Å, b = 83 Å, γ = 91°). The twofold axes perpendicular to the membrane plane are indicated. Zero and negative contours are shown as dotted lines.

virtually identical in the projection structures (Fig. 5). The 6-Å map shows a band of density going through the molecule that is flanked by two peaks on one side and one peak on the other. The arrangement of density in all rhodopsin maps is different from that in bacteriorhodopsin; however, the densities are aligned for comparison (Fig. 5).

DISCUSSION

The two-dimensional crystals of frog rhodopsin were made by extracting rod outer segment disc membranes with Tween detergents (19). Tween extractions were used in early rhodopsin purification to remove protein associated with photoreceptor membranes and was shown not to affect the retinal chromophore (26). With Tween 80 we obtained tubular membrane structures (Fig. 1 A and C) with a $p2$ lattice (Fig. 2 A and C) in which all molecules are oriented in the same direction as

Table 4. Comparison of three rhodopsin crystal forms

	$p222_1$ bovine	$p22_12_1$ frog	$p2$ frog
a, Å	43	40	32
b, Å	140	146	83
γ, degrees	90	90	91
Molecules per unit cell	4	4	2
Area per molecule, Å^2	1505	1460	1328

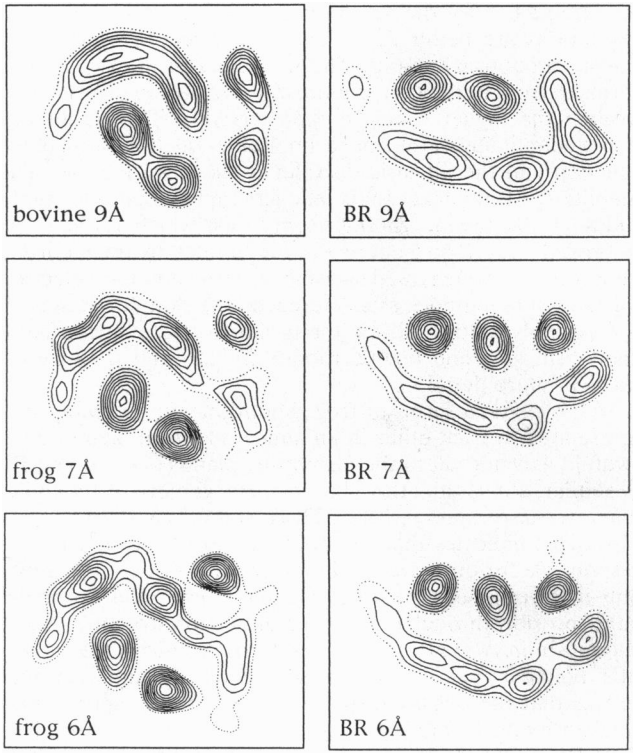

FIG. 5. Comparison of frog with bovine rhodopsin and bacteriorhodopsin (BR). The projection density for a bovine rhodopsin molecule at 9 Å and for a frog rhodopsin molecule at 7 Å from the $p22_12_1$ map and at 6 Å from the $p2$ map are shown. Bacteriorhodopsin molecules at 9-Å, 7-Å, and 6-Å resolution are shown with the same contour levels and at the same scale. Negative contours were omitted and the zero contour is represented by a dotted line.

expected for a crystal derived by extraction of lipids from disc membranes. In the $p22_12_1$ form favored in the presence of Tween 80 and Tween 20 (Fig. 1 B and D; Fig. 2 B and D), half the molecules were upside down in the membrane due to twofold screw axes in the membrane plane. This indicates either that the protein had been solubilized or that membrane fusion had occurred during the preparation. The present $p22_12_1$ crystal form is the same as that obtained previously (19). However, the arrangement of the molecules in both crystals is different from the previously reported $p222_1$ crystals of bovine rhodopsin, which were prepared from detergent-solubilized, purified bovine rhodopsin by adding lipids and removing the detergent by dialysis (18). Both $p22_12_1$ and $p2$ crystals form a higher proportion of vesicles than the bovine $p222_1$ crystals and they diffract to higher resolution. The phase errors of the unique Fourier components after averaging showed that phases were reliable to a resolution of 7 Å for the

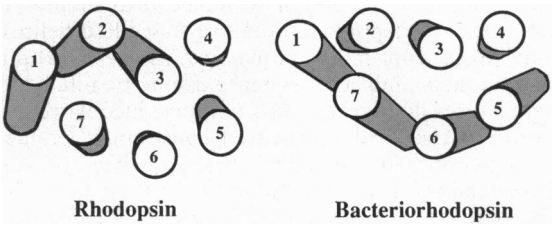

FIG. 6. Tentative arrangement of the seven helices in rhodopsin and bacteriorhodopsin. Bacteriorhodopsin consists of three helices nearly perpendicular to the membrane plane (helices 2–4) arranged parallel to a row of four tilted helices (nos. 1, 7, 6, and 5). In rhodopsin a band of four tilted helices (nos. 1–3 and 5) runs through the molecule with two nearly perpendicular helices on one side (nos. 7 and 6) and one helix on the other side (no. 4).

$p22_12_1$ to a 6 Å for the $p2$ crystal form (Fig. 3 *A* and *B*). Both resolutions are better than the 9 Å previously reported for bovine rhodopsin crystals. The molecules in the two crystal forms of frog rhodopsin are more densely packed, which could explain the higher order of these crystals. The resolution-dependent fading of the image amplitudes due to the envelope function and the intrinsic disorder is shown in Fig. 3*C*. The amplitudes of the $p2$ crystals fade less rapidly than the amplitudes of the bovine rhodopsin crystals, which reflects the improved order. To restore the amplitudes to their correct level, the data were scaled by using bacteriorhodopsin electron diffraction amplitudes as a reference (18). Amplitude scaling was recently used to obtain three-dimensional maps of halorhodopsin (24) and bovine rhodopsin (25) and is discussed there in more detail.

In both crystal forms of frog rhodopsin, pairs of molecules are related to each other in an almost identical manner by a twofold axis normal to the membrane plane (Fig. 4 *A* and *B*). A similar, almost identical dimeric arrangement of the molecules was also found in the $p222_1$ crystal of bovine rhodopsin (18). This indicates that the pointed end of the molecule is responsible for dimerization in the crystal. The contact probably involves a helix–helix interaction between the two molecules, possibly through helix 1. The projection structure of frog rhodopsin in two different crystal forms confirms the molecular boundary chosen for bovine rhodopsin and therefore proves that the density displayed in Fig. 5 corresponds to a single rhodopsin molecule. All distances between resolved features within the molecule are nearly identical in all three maps. The structures of bovine and frog rhodopsin are very similar, as one would expect from the 85% sequence identity of frog opsin sequence with that of bovine opsin (27). The use of highly purified bovine rhodopsin to produce crystals showing a very similar structure proves beyond doubt that the identity of the molecules seen with the Tween extraction procedure is anything other than frog rhodopsin (18, 19). Furthermore, the similarity of the three projection structures shows that two-dimensional crystallization conditions did not affect either the overall structure or its tilt in the membrane.

Vertebrate rhodopsins are G protein-coupled light receptor proteins that bind 11-*cis*-retinal, whereas bacteriorhodopsins are light-driven archebacterial proton pumps that use all-*trans*-retinal. Comparison of projection maps of frog and bovine rhodopsin with bacteriorhodopsin at equivalent resolution (Fig. 5) indicates that the arrangements of the seven helices in the two molecules are clearly different, as expected from the absence of sequence homology between the two families. Rhodopsin in cross-section appears more compact, bacteriorhodopsin more elongated. The bacteriorhodopsin projection shows three peaks of density corresponding to three vertical helices which are surrounded by an arc of overlapping densities of four tilted helices. The frog rhodopsin projections show three distinct peaks of density arranged as a triangle which correspond to three vertical helices and a band of density extending through the center of the molecule that is most likely caused by the overlapping densities of four tilted helices.

From projection maps alone the seven hydrophobic stretches in the amino acid sequence cannot be related to the density features in the maps. In a tentative model, we use the numbering derived from structural constraints obtained by comparing G protein-coupled receptor sequences (6). A schematic drawing consistent with all present data is shown in Fig. 6. Three of the seven helices, possibly helices 1–3, are tilted and overlap in projection, whereas helices 4, 6, and 7 are perpendicular to the membrane plane. Helix 5 appears as a peak in the bovine 9-Å map and as an elongated feature pointing toward helix 4 in the 7-Å $p22_12_1$ and the 6-Å $p2$ frog rhodopsin map. Helix 5 is, therefore, likely to be more tilted than helices 4, 6, and 7. However, angle and direction of tilts can be obtained only from three-dimensional analysis. The higher order of the frog rhodopsin crystals brings us closer to a three-dimensional map of rhodopsin which will help us to understand the mechanism of action not only of rhodopsin but of G protein-coupled receptors in general.

We thank Richard Henderson for help with amplitude scaling, Claudio Villa for preparing the $p22_12_1$ crystals, Hugh McDowell for assistance, and Gabriella Frigerio for reading the manuscript. This work was supported by Grant EY06226 from the National Institutes of Health and by an award from Research to Prevent Blindness, Inc. (to P.A.H.).

1. Hargrave, P. A. & McDowell, J. H. (1992) *Int. Rev. Cytol.* **137B,** 49–97.
2. Khorana, H. G. (1992) *J. Biol. Chem.* **267,** 1–4.
3. Ovchinnikov, Y. A., Abdulaev, N. G., Feigina, M. Y., Artamonov, I. D., Zolotarev, A. S., Kostina, M. B., Bogachuk, A. S., Miroshnkov, A. I., Martinov, V. I. & Kudelin, A. B. (1982) *Bioorg. Khim.* **8,** 1011–1014.
4. Hargrave, P. A., McDowell, J. H., Curtis, D. R., Wang, J. K., Juszczak, E., Fong, S. L., Rao, J. K. M. & Argos, P. (1983) *Biophys. Struct. Mech.* **9,** 235–244.
5. Nathans, J. & Hogness, D. S. (1983) *Cell* **34,** 807–814.
6. Baldwin, J. M. (1993) *EMBO J.* **12,** 1693–1703.
7. Baldwin, J. M. (1994) *Curr. Opin. Cell Biol.* **6,** 180–190.
8. Hargrave, P. A. (1977) *Biochim. Biophys. Acta* **492,** 83–94.
9. Karnik, S. S., Ridge, K. D., Bhattacharya, S. & Khorana, H. G. (1993) *Proc. Natl. Acad. Sci. USA* **90,** 40–44.
10. Ovchinnikov, Y. A., Abdulaev, N. G. & Bogachuk, A. S. (1988) *FEBS Lett.* **230,** 1–5.
11. Karnik, S. S. & Khorana, H. G. (1990) *J. Biol. Chem.* **265,** 17520–17524.
12. Davidson, F. F., Loewen, P. C. & Khorana, G. H. (1994) *Proc. Natl. Acad. Sci. USA* **91,** 4029–4033.
13. Bownds, D. (1967) *Nature (London)* **216,** 1178–1181.
14. Oprian, D. D. (1992) *J. Bioenerg. Biomembr.* **24,** 211–217.
15. Chabre, M. (1985) *Annu. Rev. Biophys. Biophys. Chem.* **14,** 331–360.
16. Shichi, H. & Shelton, E. (1974) *J. Supramol. Struct.* **2,** 7–16.
17. Chabre, M. (1978) *Proc. Natl. Acad. Sci. USA* **75,** 5471–5474.
18. Schertler, G. F. X., Villa, C. & Henderson, R. (1993) *Nature (London)* **362,** 770–772.
19. Corless, J. M., McCaslin, D. R. & Scott, B. L. (1982) *Proc. Natl. Acad. Sci. USA* **79,** 1116–1120.
20. Dubochet, J., Adrian, M., Chang, J. J., Homo, J. C., Lepault, J., McDowell, A. W. & Schultz, P. (1988) *Q. Rev. Biophys.* **21,** 129–228.
21. Valpuesta, J. M., Carrascosa, J. L. & Henderson, R. (1994) *J. Mol. Biol.* **240,** 281–287.
22. Amos, L. A., Henderson, R. & Unwin, P. N. T. (1982) *Prog. Biophys. Mol. Biol.* **39,** 183–231.
23. Henderson, R., Baldwin, J. M., Downing, K. H., Lepault, J. & Zemlin, F. (1986) *Ultramicroscopy* **19,** 147–178.
24. Havelka, W. A., Henderson, R. & Oesterhelt, D. (1995) *J. Mol. Biol.* **247,** 726–738.
25. Unger, V. M. & Schertler, G. F. X. (1995) *Biophys. J.* **68,** 1776–1786.
26. Sale, G. J., Towner, P. & Akhtar, M. (1977) *Biochemistry* **16,** 5641–5649.
27. Pittler, S. J., Fliesler, S. J. & Baehr, W. (1992) *FEBS Lett.* **313,** 103–108.